Composite Structures xxx (2014) xxx–xxx

Contents lists available at ScienceDirect

Composite Structures

journal homepage: www.elsevier.com/locate/compstruct

Retrofitting of interior RC beam–column joints using CFRP strengthened SHCC: Cast-in-place solution

Esmaeel Esmaeeli [a,*], Joaquim A.O. Barros [a], Jose Sena-Cruz [a], Luca Fasan [b], Fabio Raimondo Li Prizzi [b], José Melo [c], Humberto Varum [d]

[a] ISISE, Dept. Civil Eng., University of Minho, Guimarães, Portugal
[b] Dept. Civil Eng., University of Padova, Padova, Italy
[c] Dept. Civil Eng., University of Aveiro, Portugal
[d] Dept. Civil Eng., University of Porto, Portugal

ARTICLE INFO

Article history:
Available online xxxx

Keywords:
Strain hardening cementitious composite (SHCC)
Carbon fiber reinforced polymer (CFRP)
Hybrid composite plate (HCP)
Interior reinforced concrete (RC)
beam–column joint
Cyclic behavior
Retrofitting

ABSTRACT

The effectiveness of a repair strategy, for damaged RC beam–column joints, that combines strain hardening cementitious composite (SHCC) and laminates of carbon fiber reinforced polymers (CFRP laminates) is assessed in the present work. According to this technique, existing concrete cover in the joint zone of the frame is replaced by a self-compacting SHCC. This thin layer of SHCC is reinforced with CFRP laminates that are bonded into the saw cut grooves. Two full-scale severely damaged interior RC beam–column joints were retrofitted using two different configurations for this technique: (i) applying the strengthening system in the front and rear faces of the specimens; (ii) jacketing all sides of the elements of the specimens with the strengthening system. The effectiveness of these retrofitting configurations are assessed and compared by evaluating experimentally the hysteretic response, the dissipated energy, the degradation of secant stiffness, the displacement ductility and the failure modes of each repaired specimen, and also using the values of these indicators obtained in the virgin state of these specimens. This comparison revealed that the adopted retrofitting strategies can restore and even enhance the performance of this type of structural elements, mainly when the solution based on four-sided jacketing is used.

1. Introduction

Seismic deficiencies of RC structures designed based on pre-seismic provisions, such as pre-1970th buildings, is figured out in both experimental tests [1,2] and also post-earthquake observations (e.g. Turkey 1999 and Italy 2009). These vulnerabilities are mostly due to the lack of seismic design and detailing of these structures. Among the structural components of a framed-structure, beam–column joints play the most significant role in the lateral stability, since a brittle failure at the joint region may result in a progressive collapse of a building. Therefore, both energy dissipation and ductility capacities of these structures, when a seismic event occurs, highly depend on the stability and deformation of the beam–column joints. Continuous damage due to aging effects, even in those structures designed based on seismic oriented codes, also makes them vulnerable against earthquakes.

Several strategies for seismic retrofitting of these group of structures are available, such as steel jacketing, cast-in-place concrete/RC jacketing [3], shotcrete jacketing [4], epoxy injection repair [5], application of Fiber Reinforced Polymers (FRPs) [6–9].

Li et al. [10] showed that the interior RC beam–column joints can be strengthened by using a ferrocement jacket as the replacement of the exiting concrete cover at critical regions of the framed elements along with embedding inclined bars in the joint region. High performance fiber reinforced composites (HPFRC) were used by Shannag and Alhassan [11] for the strengthening of 1/3 scale interior beam–column joints containing vulnerable detailing against seismic actions. A 25 mm thick jacket of HPFRC covering critical regions of column-joint and extending up to a 100 mm on the beams of the specimens were the adopted strengthening configuration. The results of this experimental program have revealed that HPFRC jackets can significantly improve the seismic response of deficiently detailed interior beam–column joints. However, this

* Corresponding author at: ISISE, Dep. Civil Eng., School Eng., University of Minho, Campus de Azurém, 4800-058 Guimarães, Portugal. Tel.: +351 917 40 90 75.
E-mail addresses: esmaeeli_civil@outlook.com (E. Esmaeeli), barros@civil.uminho.pt (J.A.O. Barros), jsena@civil.uminho.pt (J. Sena-Cruz), morefasan@gmail.com (L. Fasan), fabioliprizzi@gmail.com (F.R. Li Prizzi), josemelo@ua.pt (J. Melo), hvarum@fe.up.pt (H. Varum).

http://dx.doi.org/10.1016/j.compstruct.2014.12.012
0263-8223/

jacketing solution has increased the dimensions of the cross sections of the elements in 25% to 47%, which can be a real obstacle on the use of this technique in certain applications. The experimental program performed by Tsonos [4] was focused on the strengthening of 1/2 scale exterior beam–column joints by adding a new steel cage reinforcement that was covered either with shotcrete or cast-in-place cement based materials. Based on the results of this experimental program, Tsonos [4] stated that both cast-in-place and shotcrete solutions provided a significant improvement in the seismic response of this type of structures. A superior performance of the cast-in-place solution in respect to the shotcrete technique, mainly in terms of energy dissipation capacity, was observed and attributed to a better covering of the added steel bar cage that was assured by the former technique. Considering an increase of 140 mm in each side of the column's cross section of the 1/2 scale specimens, inacceptable interference can result in terms of architectural and functional requisites. Wang and Hsu [12] a satisfactory performance of the strengthening effectiveness of RC jacketing of columns of beam–column assemblies with shear deficiency in the joint region. For this case, the adopted thickness of the RC jacket resulted in an increase up to 67% in the dimensions of the column section.

Strain hardening cementitious composite (SHCC) is a class of Fiber Reinforced Concretes (FRCs), with the character of developing a continuous increase of post-cracking tensile capacity up to the stress localization at one of the multiple formed cracks for a relatively high tensile strain. The formation of multiple diffused hairline cracks through all the loaded length of the specimen during the hardening stage assures levels of ductility not possible to attain in conventional FRCs. By testing in bending masonry elements strengthened with a thin layer of SHCC applied to their tensile face, Esmaeeli et al. [13] demonstrated that higher load carrying capacity and ductility is achievable when compared to flexural strengthening methodologies based on the use of thicker layers of self-compacting steel FRC. Recently Esmaeeli et al. [14] developed a thin prefabricated hybrid composite plate (HCP), composed of SHCC and CFRP laminate, with a high durability potential. By performing some experimental tests, they demonstrated the high efficacy of the HCP for the repair and the strengthening of the different types of the RC elements including retrofitting of damaged beam–column joints.

In this paper an experimental program for the assessment of the effectiveness of a retrofitting technique for damage interior RC beam–column joints by casting-in-place SHCC and further reinforcing that with CFRP laminates is described, and the main obtained results are presented and discussed.

Both the fine graded matrix and the high content of fly ash in the skeleton of SHCC can promote the formation of a relatively high bond quality at the interface between SHCC and existing concrete. A high strain capacity (strain at maximum tensile strength of composite) and a tight crack width, often and in average smaller than 100 μm up to the ultimate tensile capacity, is known as a durable composite cover and expected sufficient confining pressures at relatively high strains. In fact, the results of previous studies showed that for the concrete patched with SHCC, a single crack with a large width formed in substrate transforms to a multiple diffused fine crack in the patch layer which are typically impermeable and assure the durability of the repaired substrate [15–17]. When SHCC is used to repair RC elements with progressive corrosion of their steel rebars, the risk of splitting and spalling of this ductile retrofitting cover due to the expanded volume of the rusted bars is minimized [18,19]. Moreover, the tensile strain ductility of SHCC results in a high potential of stress redistribution at the bearing zones, therefore avoids premature failure at this region when anchors used to enhance shear stress transference between the retrofitted layers.

The idea of reinforcing SHCC layer with bonded CFRP laminates into the saw cut grooves benefits the progressive increase in tensile strength of the SHCC, at least up to the rupture strain of CFRP laminate, generally 1.5% to 1.6%. This provides strain compatibility between these two composites while ductility of SHCC in combination of high tensile strength of CFRP laminates may produce a strengthening scheme with a high toughness. Also bonding CFRP laminates as the supplementary tensile reinforcement to the exposed face of the SHCC layer, in the hardened state, minimizes the obstacles during placing the fresh SHCC. A better bond quality control between SHCC and CFRP laminates can be expected too. Finally, the mechanism of formation of numerous diffused micro cracks and opening and closing of those during reversal cyclic loads results in a high capacity of energy dissipation which is the most desired character for seismic load resisting elements.

2. Experimental program

The experimental program is composed of retrofitting two severely damaged full-scale interior beam–column joints. The retrofitting methodology was based on replacing concrete cover with SHCC in the joint region and along the critical lengths of beams and columns. To enhance the tensile strength of this ductile layer, CFRP laminates were bonded into grooves cut on hardened SHCC along both the longitudinal and the transverse directions. Two different depths, 10 and 20 mm, for the grooves were adopted in order to allow the arrangement of the CFRP laminates in two different orientations. An X-shaped configuration of these CFRP laminates, bonded in two different levels, was used for the shear strengthening of the joint region.

The difference between the adopted retrofitting schemes for the tested specimens was the number of faces of the framed elements that was retrofitted. While in one specimen only the front and rear faces of beams, columns and joint were retrofitted, for the other specimen all the external faces of the mentioned elements were jacketed.

After retrofitting, these specimens were subjected to the same test setup and loading pattern that were used to characterize their lateral load–displacement response in their virgin state. To evaluate the efficacy of the adopted retrofitting strategies the results obtained from these experiments were then compared to the corresponding results of their virgin states.

2.1. Damaged specimens

Two severely damaged interior RC beam–column joints, designated as JPA3 and JPB, were selected from a group of specimens that were tested in their virgin state in the ambit of an experimental research program of a PhD thesis [20]. Both specimens were identical in terms of the lengths and cross section geometry of their framed elements. The only difference between these specimens was the number of longitudinal rebars: more 4 longitudinal rebars were used in the column of JPB. The lengths of the beams and columns of these specimens were taken as the mid-span and the mid-storey of a common RC building built before 1970th, respectively. The mid-length of the elements were used to facilitate the simulation of the boundary conditions in the experimental test since moment inflection point of a RC frame under a lateral loading is expected to occur in the these zones.

According to the configuration of the most buildings constructed before 1970th, plain steel bars were used as the longitudinal and transverse reinforcement for both beams and columns. There were no transverse reinforcement in the joint region and 90° bended end was used for the stirrups and hoops of the beams and columns, respectively. More details about the configuration of the selected specimens for the retrofit, JPA3 and JPB, are shown in

Please cite this article in press as: Esmaeeli E et al. Retrofitting of interior RC beam–column joints using CFRP strengthened SHCC: Cast-in-place solution. Compos Struct (2014), http://dx.doi.org/10.1016/j.compstruct.2014.12.012

Fig. 1. Adopting a shorter length for the inferior column was due to the limitation imposed by the test setup which is discussed further in this section.

The average compressive strength, measured in 150 mm cubes of concrete, was equal to 23.8 MPa with an estimated characteristic compressive strength of 19.8 MPa, corresponding to the C16/C20 concrete strength class according to the classifications of the EC2-1992-1-1 [21]. By performing tensile tests, average values of 590 and 640 MPa were determined for the yield and the ultimate tensile strength of the steel longitudinal reinforcement, respectively, with an elasticity modulus of 198 GPa.

A lateral reversal displacement history was imposed to the top of the superior column at the presence of a constant axial load of 450 kN. This axial force introduces a gravity load corresponding to an axial compressive stress of 21.3% of the average concrete compressive strength. The lateral load was constituted of a series of displacement-controlled cycles, in push (positive displacement) and pull (negative displacement) direction, with an incremental

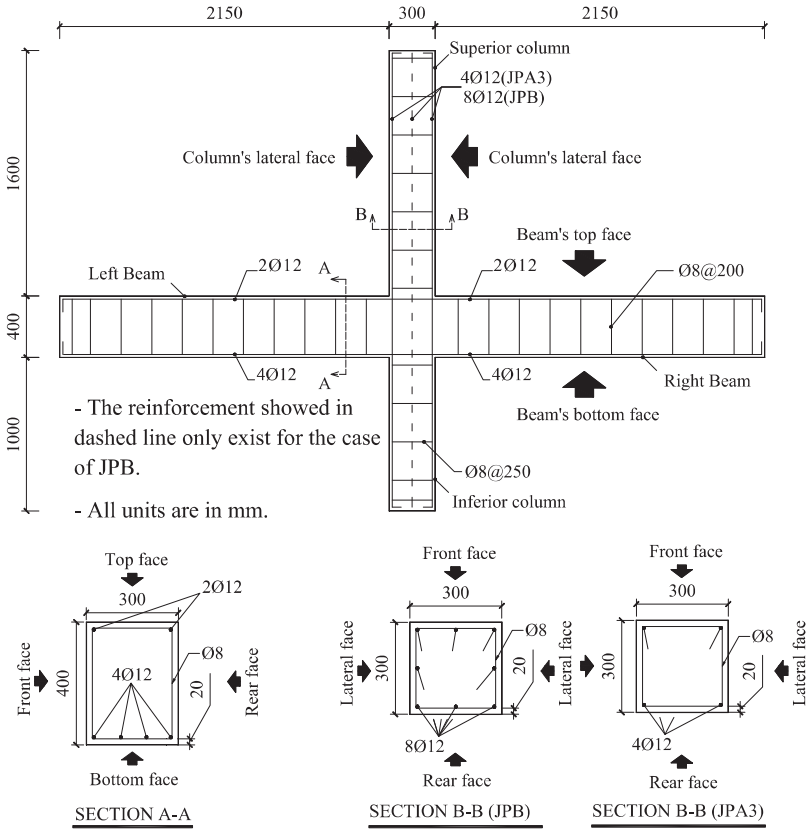

Fig. 1. Details of adopted configurations for the interior RC beam–column connections.

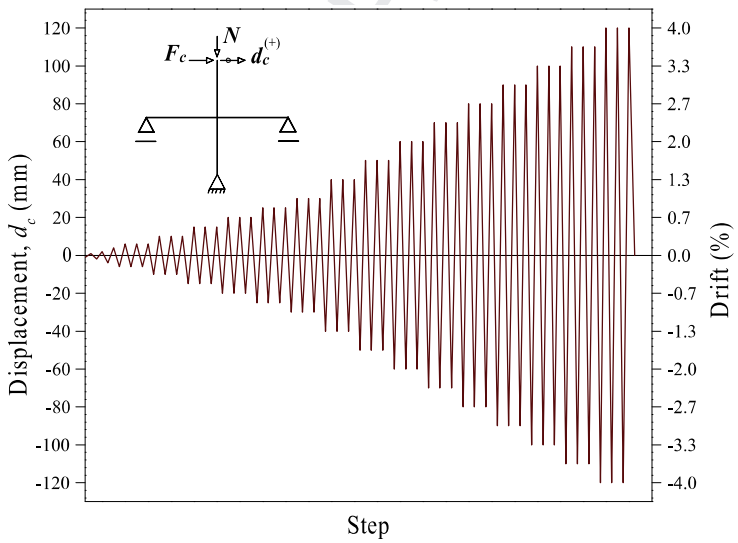

Cycle Numbers	d_c^p (mm)	Max drift (%)
1	±1	0.033
2	±2	0.067
3	±4	0.133
4 to 6	±6	0.20
7 to 9	±10	0.33
10 to 12	±15	0.50
13 to 15	±20	0.67
16 to 18	±25	0.83
19 to 21	±30	1.00
22 to 24	±40	1.33
25 to 27	±50	1.67
28 to 30	±60	2.00
31 to 33	±70	2.33
34 to 36	±80	2.67
37 to 39	±90	3.00
40 to 42	±100	3.33
43 to 45	±110	3.67
46 to 48	±120	4.00

Fig. 2. Loading history adopted for the lateral displacement cycles (d_c^p: peak displacement for the corresponding cycle or set of cycles).

magnitude up to 4% interstory drift. After three cycles of loading that introduced a drift level of 0.13%, each level of displacement was repeated three times, as it is shown in Fig. 2. The specimens were tested in a horizontal position according to the test setup illustrated in Fig. 3. As it is shown in this figure, the shorter length of the inferior column of the specimen is connected to a steel element with equivalent stiffness, to accommodate the load cells and pin connection at the bottom of this column.

The maximum load carrying capacity of 43.2 and 39.5 kN was registered for JPA3 and JPB, respectively, at the drift levels of 2.7% and 2.3%, correspondingly.

As shown in Fig. 4, in both specimens the extents of the damages included concrete crushing and spalling at the intersections of the beams and the columns, and sever sliding of longitudinal reinforcement due to significant bond deterioration. Flexural cracks on the right beam of both specimens were localized at the beam–joint interface. The main crack at the right beam of JPA3 and JPB specimens is at a position of 120 and 170 mm far from beam–joint interface, respectively. There were minor flexural cracks at the column-joint interfaces of JPB. Specimen JPA3 also has experienced severe damages concentrated in the joint region, where two wide diagonal cracks have formed and concrete cover has spalled. Additional information about experimental program and test results of the virgin specimens can be found elsewhere [20].

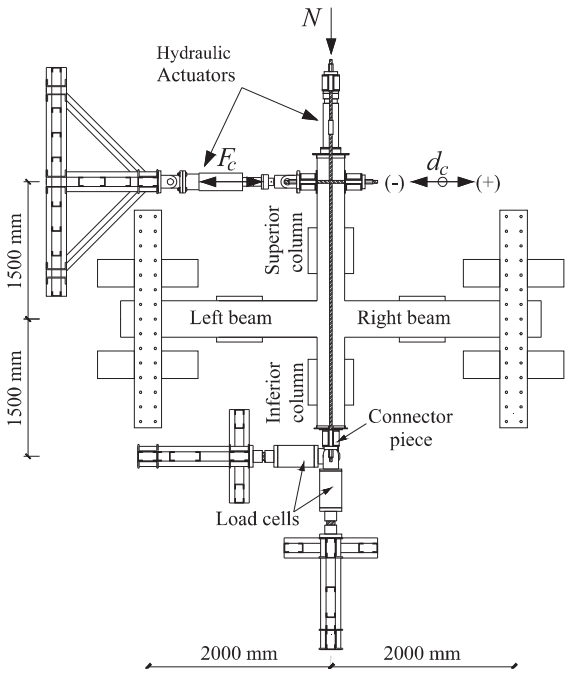

Fig. 3. Test setup adopted for the horizontally placed specimens [20].

2.2. Retrofitting strategy

According to the adopted retrofitting strategy, the concrete cover at critical regions of the damaged beam–column joints is replaced with a thin layer of a casted-in-place SHCC. Afterward, this layer of the SHCC was reinforced with CFRP laminates bonded to the saw cut grooves on that according to the NSM technique. Chemical anchors were used to improve inter-laminar shear stress transference between the SHCC and the concrete substrate. The rheology of the SHCC material, used in this study, is tailored to produce a highly fluid and self-compacting fresh state behavior so that this composite can easily flow and fill narrow spaces between the formworks and the existing concrete (gaps of less than 25 mm).

To the retrofitted JPA3 and JPB specimens, the nomination of the JPA3-R and JPB-R was attributed, respectively. As mentioned before, the adopted retrofitting schemes for the specimens differed according to the number of faces of their elements which was retrofitted. While in JPA3-R only the front and rear faces of beams, columns and joint were retrofitted, in JPB-R all the external faces of the mentioned elements were jacketed.

The retrofitting process was applied with the specimens positioned horizontally and in two steps: (i) before and (ii) after turning the specimens. Following the details of each step of the retrofitting strategy are described.

2.2.1. Concrete cover removal and replacement

Details of the retrofitting schemes are presented in Fig. 5. The retrofitting length for both beams and columns was taken as twice of the section depth of the corresponding element. Therefore, using a jackhammer concrete cover was removed in the joint region and also in all lateral faces of the beams and columns of both specimens for a length of 800 and 600 mm, respectively. The concrete cover was initially removed up to a depth to expose the longitudinal reinforcements. Afterward, in an effort of increasing the interface area between casted-in-place materials and existing steel bars, the removal of the concrete cover continued up to attain approximately half of the diameter of the longitudinal bars. To seal the existing cracks, boreholes were drilled through the cracked sections. After cleaning the holes using compressed air, small diameter pipes were placed inside them, then the exposed crack development at the concrete substrate was sealed and epoxy resin SikaDur-52 was injected. After turning the specimen, the injection was repeated to assure that the cracked section was sealed as much as possible.

Wooden formworks with interior varnished faces were installed to cast the cement based materials. The lateral faces of columns and the top and bottom faces of the beams of JPA3 were casted using a mortar that was then cured for 7 days (see Fig. 1 for the nomination of the faces of the elements of the beam–column

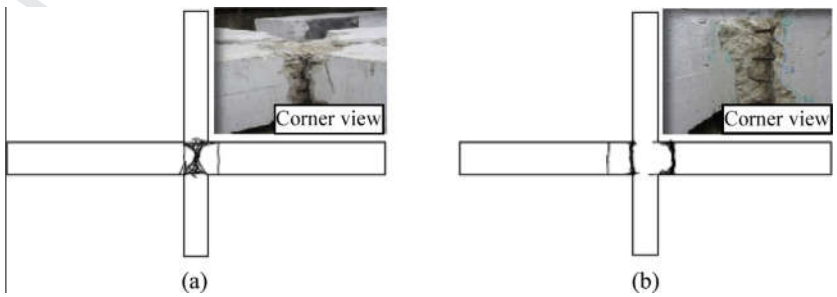

Fig. 4. The extent of damages before retrofitting (a) JPA3 and (b) JPB.

Please cite this article in press as: Esmaeeli E et al. Retrofitting of interior RC beam–column joints using CFRP strengthened SHCC: Cast-in-place solution. Compos Struct (2014), http://dx.doi.org/10.1016/j.compstruct.2014.12.012

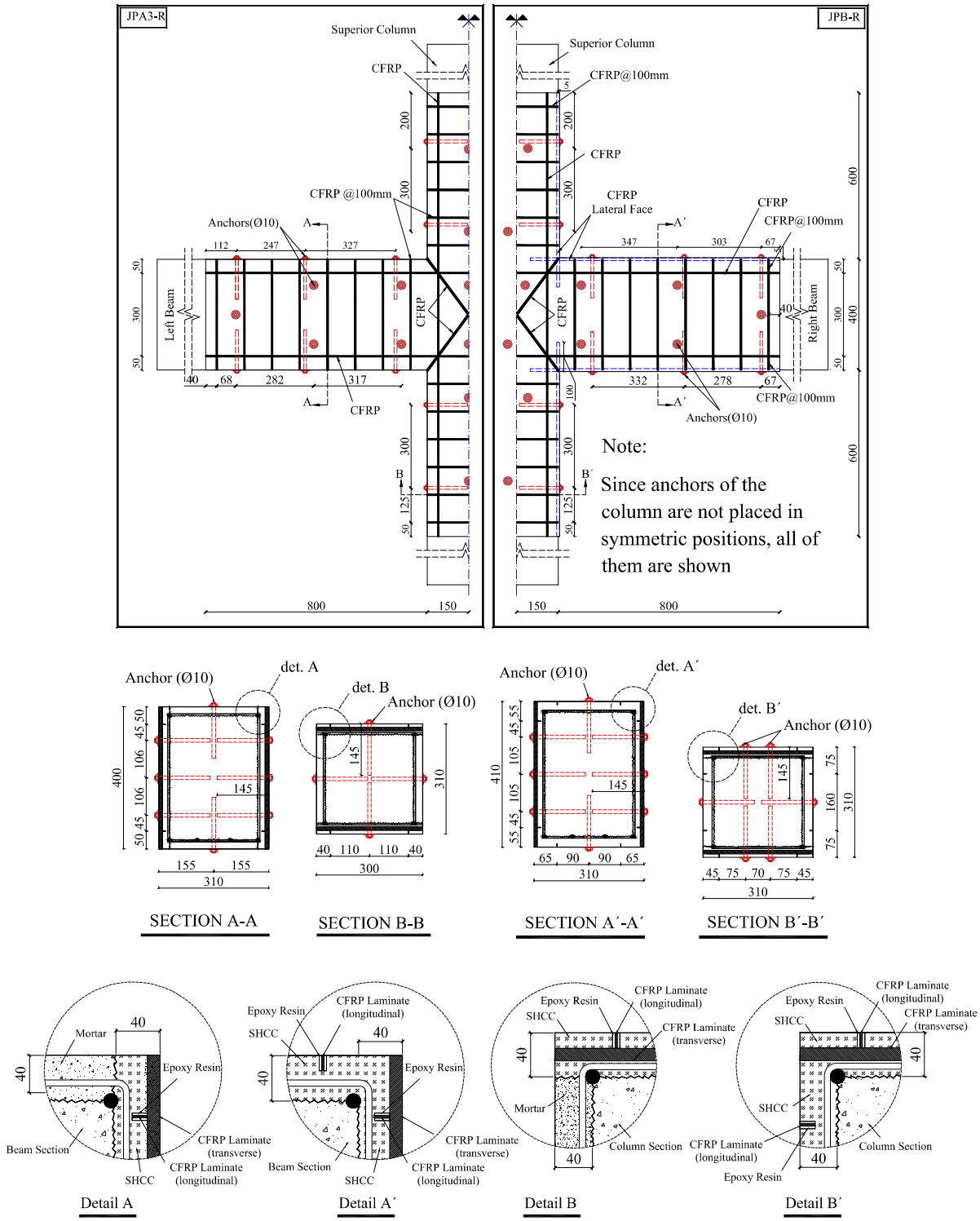

Fig. 5. Details of the schemes used for the retrofitting of the damaged specimens (dimensions in mm).

joints). After this period of curing, the top edges of the hardened mortar were roughened and fresh SHCC was placed.

For the case of JPB, a continuous placing of SHCC starting from lateral faces of the columns and the top and bottom faces of the beams, and then moving to the front face of the specimen was followed.

Considering the variation in the thickness of the existing concrete cover, between 16 and 20 mm, and a minimum of 20 mm thickness required to accommodate two layers of CFRP laminates in the SHCC layer, a 5 mm higher finishing level for the SHCC was adopted, as measured from the level of the existing concrete cover at the extremities of the retrofitted regions.

The self-compacting character of the SHCC and its high fluidity eliminated the need to any external vibration. Only the exterior face of the fresh SHCC was levelled by using a thin long metal bar, with a rectangular cross section, for the finishing purpose.

Please cite this article in press as: Esmaeeli E et al. Retrofitting of interior RC beam–column joints using CFRP strengthened SHCC: Cast-in-place solution. Compos Struct (2014), http://dx.doi.org/10.1016/j.compstruct.2014.12.012

Fig. 6. View of the retrofitted specimens (a) JPA3-R and (b) JPB-R.

It should be noted that before casting the cement based materials, the concrete substrate was saturated with water in order to assure a better interface bond and a lower risk of developing shrinkage cracks.

One day after casting the SHCC the formworks were removed. A wet curing procedure was followed for at least 7 days as it was reported the most appropriate curing for SHCC [22]. After at least 17 days of casting the SHCC, grooves were executed on the SHCC according to the configurations showed in Fig. 5. These grooves had 5 mm of width, and 10 or 20 mm of depth, depending on the level adopted for the installation of the CFRP laminates. Before inserting the CFRP laminates, the grooves were cleaned by using compressed air, and then filled with epoxy resin S&P 220 as the bonding agent. Afterward, CFRP laminates that were previously cleaned with acetone, were placed inside the grooves.

After turning the specimens the same retrofitting process was applied to the rear face, namely: removal of the concrete cover, sealing of the cracks, roughening the top edges of newly casted materials, placing the fresh SHCC, curing of SHCC, cutting the grooves and inserting CFRP laminates.

For the case of JPB the grooves were also cut on the SHCC casted on the lateral faces of columns and the top and bottom faces of the beams, and pair of CFRP laminates was bonded into these grooves according to Fig. 5. Therefore, for the case of JPA3-R, the longitudinal reinforcement comprised pairs of continuous laminates on each of the front and rear faces of the beams and columns (see Fig. 5), while JPB had a similar CFRP strengthening but also with extra pairs of CFRP laminates bonded to the each of the lateral faces of its columns, and the top and bottom faces of its beams. CFRP laminates bonded to the lateral faces of the beams and columns were continued beyond the interface of these elements with the joint region, where the occurrence of the largest bending moments is expected (moment critical sections). For this purpose, an inclined drilling was used to execute the holes. After placing the CFRP laminates, the epoxy resin was injected. The bond length of 100 mm was adopted for these CFRP laminates after moment critical section (anchorage length), since a minimum of 90 mm is characterized as the required bonding length to fully mobilize potential tensile strength of this type of CFRP laminates [23].

The adopted spacing for transverse CFRP laminates in both JPA3-R and JPB-R was 100 mm (Fig. 5). In an attempt to increase the shear resistance of the joint region, a pair of CFRP laminates with an X shape configuration was applied on each front and rear face of the joint region of both specimens.

2.2.2. Installing chemical anchors

Chemical anchors were installed before and after turning the specimens, when the SHCC was cured at least 20 days. These 10 mm diameter anchors (HIT-V-8.8 M10X190) were mounted inside the holes perforated on the beams, columns and on the joint region, at the positions represented in Fig. 5. Before mounting the anchors, the holes were partially filled with Hilti Hit-HY 200-A, which is a fast curing injectable bonding agent. An embedded length of 145 mm was assured for the anchors, measured from the finished surface of SHCC. A torque of 30 $N \cdot m$ was applied to fasten the nuts and partially confine the concrete substrate. Fig. 6 shows a view of the specimens after have been repaired.

2.3. Material properties of retrofitting system

The self-compacting SHCC was composed of a cementitious mortar reinforced with 2% of volume short discrete PVA fibers. The PVA fiber used in this study had a length of 8 mm and was produced by Kuraray Company with the designation of RECs 15×8. The average tensile stress at crack initiation and the average tensile strength of the SHCC was 2.43 and 3.35 MPa, respectively, with a minimum tensile strain capacity of 1.3%. More details on mixture ingredients, mixing process and test setup of the SHCC can be found in [10,13,22]. From uniaxial tensile tests carried out according to the recommendations of ISO 527-2:1996 [24] on seven days cured of six dumbbell-shaped S&P 220 epoxy resin, an average tensile strength of 18 MPa and average modulus of elasticity of 6.8 GPa were obtained. Tensile properties of CFRP laminate (S&P laminate CFK 150/2000) with a cross section of 1.4×10 mm^2 were characterized following the procedure proposed in ISO 527-5:2009 [25]. From the tests executed in six coupons, average values of 2689 MPa, 1.6% and 165 GPa were obtained for the tensile strength, strain at CFRP rupture and modulus of elasticity, respectively.

2.4. Test setup and loading pattern

The test setup, lateral load history and gravity load used for testing virgin specimens were adopted for testing the retrofitted specimens.

3. Results and discussion

3.1. Hysteresis response

Fig. 7 shows the hysteretic responses of both virgin and retrofitted specimens in terms of lateral load *versus* lateral displacement (and drift) registered at the top of the superior column. Both retrofitting techniques resulted in stable loops with smooth decay of load carrying capacity in the post-peak stage of the structural response. The values registered for the maximum lateral load (F_P) and its corresponding drifts (d_P) for specimens in the retrofitted and virgin states are listed in Table 1. The increase level in terms of lateral peak load after retrofitting is also indicated in this table. According to the obtained results, the retrofitting technique adopted for JPA3-R recovered up to 93% of the maximum lateral load carried out by this specimen in its virgin state, calculated as the average load in the positive and negative directions. Applying the retrofitting technique to all lateral faces of the framed

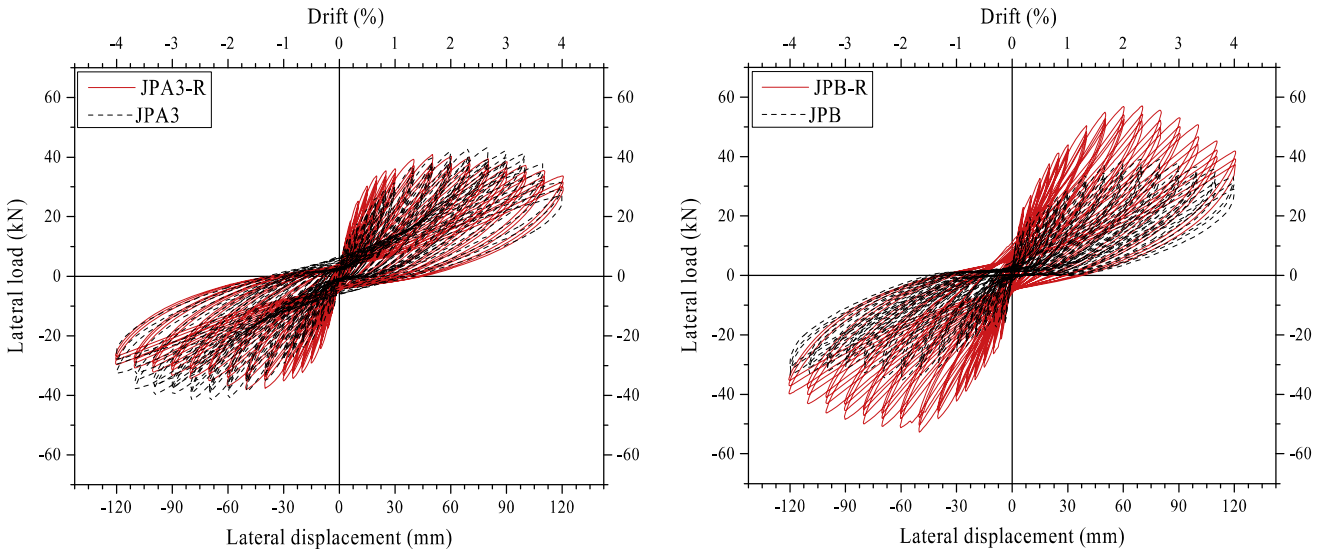

Fig. 7. Hysteretic responses of the specimens in the strengthened and virgin states.

Table 1
Maximum lateral load capacity and the corresponding drifts of the specimens in the repaired and virgin states.

Specimen	Negative direction		Positive direction		Negative direction	Positive direction
	F_p^- (kN)	d_p^- (%)	F_p^+ (kN)	d_p^+ (%)	Increase in peak load	
JPA3-R	−38.0	−1.65	+40.9	+1.65	−9.3%	−5.5%
JPA3	−41.9	−2.31	+43.3	+2.60		
JPB-R	−52.7	−1.62	+57.14	+2.33	+48.9%	+44.5%
JPB	−35.4	−1.99	+39.55	+2.24		

elements, as was done in JPB-R, resulted in a significant increase in terms of lateral load carrying capacity. This increase was +48.9% and +44.5% for negative and positive directions, respectively, when compared to the corresponding values recorded in the virgin state of this specimen (JPB).

For both strengthening techniques the average value of the drift corresponding to the maximum lateral load, in negative and positive direction, has decreased. This can be attributed to a lower shear deformation at the joint region due to the contribution of the strengthening scheme in confining the concrete of the joint core, and also in increasing the shear stiffness of the joint panel, up to the peak load.

For each specimen, the residual lateral load carrying capacity at 4% drift ($F_{4\%}$) was compared to the registered peak of the lateral load (F_p) according to $\alpha = [1 - (F_{4\%}/F_p)]\%$. The degradation of the peak load (α) was calculated for both virgin (α_v) and retrofitted specimens (α_R). The amount of this degradation was 21.85% and 25.6% for JPA3-R and JPB-R, respectively, which are the average values for negative and positive loading directions. While at the same drift level, JPA3-R had almost the same peak load degradation as JPA3 (22.35%), corresponding value for JPB-R was much higher than JPB (3.7%). Larger degradation in the peak load of JPB-R, as compared to JPB, is associated to different damage evolution and failure modes of these specimens. In fact, in comparison with JPB, JPB-R attained higher level of lateral load; therefore, higher shear stresses were applied to its joint region at the ultimate state. This resulted in an eventual damage concentration in the joint region. In the other hand, the lateral load carrying capacity of JPB was limited by the premature flexural capacity of the beams, which was caused by the sliding of their longitudinal rebars that is expected to have smoother load degradation.

3.2. Damage evolution and failure modes

Fig. 8 shows the pattern of the developed micro cracks, and major damages registered at the end of the test on the front faces of both specimens. The surface of the SHCC was painted with a transparent concrete varnish before testing the specimens. At the end of the test this surface was sprayed by a penetrating liquid to reveal micro cracks difficult to detect at necked eyes. The schematic representation of these damages is showed at the left side of the corresponding photo for the purpose of better assessment of the developed damage. The damage evolution is described in the following paragraphs.

JPA3-R: The first series of cracks has initiated at the cycles corresponding to 0.33% of drift. These cracks were formed at the top face of the left and the right beams at a distance of 100 mm from the lateral faces of the column. At cycles corresponding to 0.5% of drift, cracks at the bottom faces of both left and right beams, symmetric to the cracks on top face, were observed. Some relative sliding between retrofitting layer and concrete substrate was observed when cycles of 0.83% drift were reached.

The first series of the inclined cracks at the junction of the beams and columns was observed in all four corners at the cycles corresponding to 1% of drift. Further increase in the lateral displacement at the top of the superior column resulted in the progress of these cracks into the interface of the epoxy adhesive/SHCC of the bonded X shape CFRP system at the joint region. Thus, for any larger displacement demand, damages were localized at the joint region in the form of progressive separation between the epoxy adhesive and the SHCC. Finally, at drift cycles of 1.67%, due to the load reversal effects, the debonding was almost progressed along the entire length of the elements of the X shape CFRP

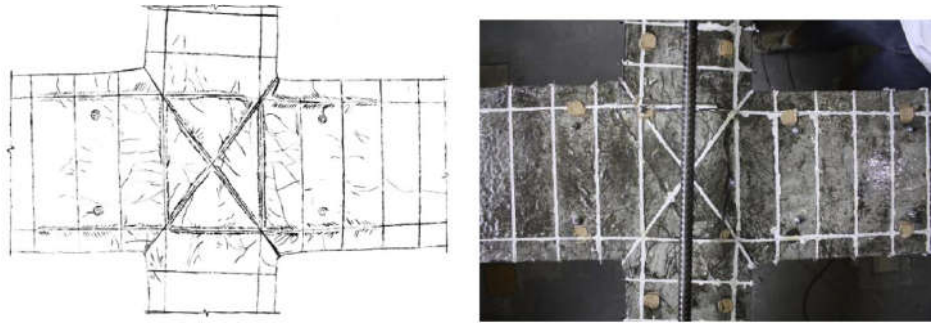

(a) JPA3-R

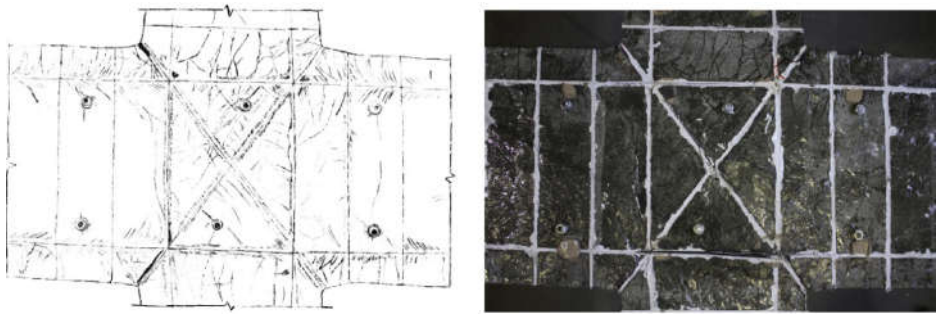

(b) JPB-R

Fig. 8. Damage propagation and concentration at the failure of (a) JPA3-R and (b) JPB-R.

configuration. As a consequence of this debonding, a total loss in contribution of these inclined CFRP laminates as a part of shear resisting mechanism of the joint region was occurred. Thus, shear failure of the joint region was the governing failure mode of JPA3-R.

JPB-R: The onset of the first series of cracks was at the set of cycles corresponding to 0.5% of drift. These cracks were formed at the top and bottom faces of the left and right beams in a distance of approximately 90 mm far from lateral faces of the column. The inclined cracks at the junction of the beams and columns were initially formed at cycles corresponding to a drift level of 0.83%. Similar to the case of JPA3-R, these set of cracks resulted in a progressive debonding along the interface of epoxy adhesive/SHCC of the X-shaped CFRP system at the joint region. At drift cycles of 1.67% this debonding was already progressed along the entire length of the inclined CFRP laminates. At the same cycles, the longitudinal steel bars at the top face of the right beam started to have significant sliding, so that the concrete cover perpendicular to the bended end of these bars was cracked. As it will be discussed in the next section, sliding of these rebars resulted in degradation of flexural capacity of the beams when the top face of them was in tension. The non-symmetrical response of JPB-R, in negative and positive loading directions, can be caused by this phenomenon. At the next sets of the cycles, corresponding to 2% of drift, the already cracked concrete cover over the bended region of these bars was spalled off. Afterward, any further increase in drift demand just followed by widening of the existing X-shaped cracks at the joint region. Therefore, the shear failure at the panel of the joint resulted in degradation of lateral load resistance of JPB-R in both negative and positive loading directions.

3.3. Flexural strength of beams

Eq. (1) represents the static equilibrium between the maximum developed moments at the left and the right beams with respect to the lateral force at the top of the column.

$$Vc = \frac{M_R - M_L}{L_c} \quad (1)$$

where Vc is the shear force in the column, M_R and M_L are the values of the internal bending moment developed at the beam–column interfaces of the right and the left beam, respectively. The sign of the bending moment is assumed positive when the bottom face of the beam is in tension and negative when this face is in compression. In Eq. (1), L_C is the total length of the column between its lateral supports (1.5 + 1.5 m). According to Eq. (1), any reduction in the flexural capacity of the left or right beams may result in the loss of lateral capacity of the beam–column assembly, unless this reduction could be compensated through the moment redistribution to other parts of the structure.

The maximum moments of each of the left and right beams *versus* the drift demands were calculated, at a distance 50 mm far from beam–column interfaces, by considering the force values registered in the load cells and equilibrium conditions, and the obtained results are illustrated in Fig. 9. Note that in this figure, for the convenience of understanding, the multiplied value of M_L by −1 is presented. Thus, the beams' bending moments corresponding to the negative and the positive loading directions are presented in the first and the third quadrants of Cartesian system, respectively.

According to Fig. 9a, the maximum bending moments developed in the left (M_L) and the right (M_R) beams of JPA3-R, during the negative displacement, were +65.94 and −39.6 kN · m both at a drift level of −1.64%. During the positive displacement, the left and the right beams reached their maximum bending moment, −43.04 and +71.17 kN · m, at drift levels of +1.65% and +2.65%, respectively.

As depicted in Fig. 9b, the values of maximum bending moments for JPB-R in the left and the right beams, during the negative displacement were +108.81 kN · m at a drift level of −2.62% and −57.16 kN · m at −1.62% of drift, respectively. The developed maximum bending moment for the positive displacement, in the left and the right beams were −55.64 and +107.46 kN · m at drift

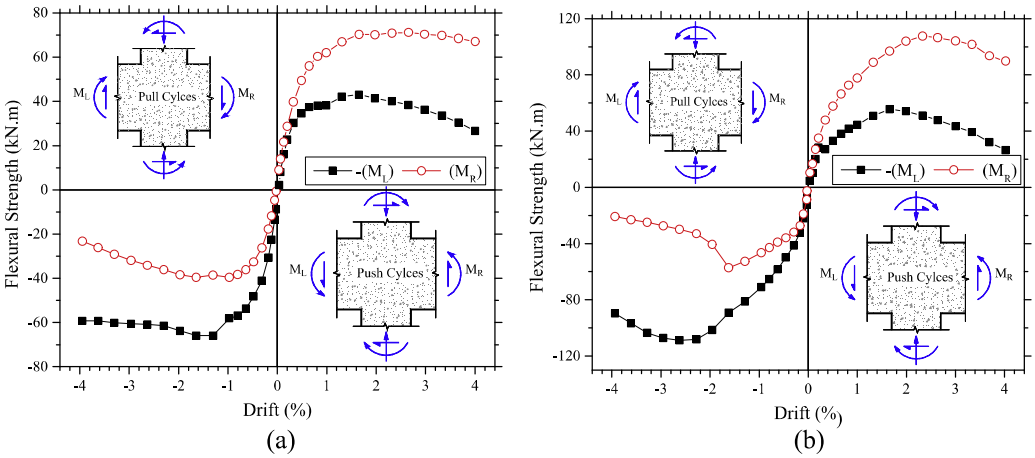

Fig. 9. Development of the resisting bending moment at the interfaces of the beams with columns (a) JPA3-R and (b) JPB-R.

Table 2
Maximum bending moments developed in the beams of the repaired and the virgin specimens.

Specimen	Negative direction		Positive direction		Negative direction		Positive direction	
	Absolute values				Variation			
	M_L^+ (kN · m)	M_R^- (kN · m)	M_L^- (kN · m)	M_R^+ (kN · m)	M_L^+	M_R^-	M_L^-	M_R^+
JPA3-R	+65.94 (−1.64)*	−39.6 (−1.64)	−43.04 (+1.65)	+71.17 (+2.65)	−13.07%	−1.39%	+8.03%	−10.98%
JPA3	+75.85 (−2.32)	−40.16 (−2.32)	−39.84 (+2.59)	+79.95 (+2.59)				
JPB-R	+108.81 (−2.62)	−57.16 (−1.62)	−55.64 (+1.66)	+107.46 (+2.33)	56.16%	79.35%	62.22%	41.81%
JPB	+69.68 (−4.0)	−31.87 (−1.99)	−34.30 (+2.58)	+75.78 (+2.44)				

* Values in parentheses indicate the corresponding drift in percentage at maximum bending moment.

levels of +1.66% and +2.33%, respectively. A sudden reduction observed in bending moment capacity of the right beam during negative loading at drift cycle of 1.67% (Fig. 9b) was caused by a significant sliding of longitudinal bars at the top face of the right beam, as discussed in the previous section.

The registered maximum bending moments for these specimens during both the positive and the negative loading displacements are also indicated in Table 2. In this table M_L^+, M_L^-, M_R^+ and M_R^- indicate the positive and negative bending moments in the left or right beams. Corresponding values for their virgin state and the percentage of the increase in their flexural capacities achieved after the retrofitting are also reported in this table. According to this data, after retrofitting, in average and for the positive bending moments, up to 88% of flexural capacity of the beams of JPA3 was recovered. For the negative bending moments, the flexural capacities of the beams in virgin state were fairly restored. The retrofitting system adopted for JPB, however, provided a much larger increase in resisting bending moments of the beams. Based on this retrofitting technique an average increase of 49% and 71% for the positive and negative moments were obtained, respectively.

It should be noted that the values registered for flexural resistance of both retrofitted specimens do not necessarily represent the flexural capacity of the beams, since the degradation in beam–column joint shear capacity was the prevailing failure modes of both specimens.

3.4. Dissipated energy

Energy dissipation capacity of a RC element is the consequence of inelastic deformation and damage propagation. Opening and closing of cracks contribute significantly to the energy dissipation capacity, as well. Therefore, for SHCC material with the potential of formation multiple diffused micro cracks, a high level of energy dissipation under cyclic loadings is expected. The amount of dissipated energy per cycle, E_i, can be calculated from the enclosed area in each loading cycle, as presented by the hysteresis response of lateral load *versus* lateral displacement. Summation of the dissipated energy with respect to the increment in lateral drift results in cumulative dissipated energy up to each given level of interstory drift. The evolution of the dissipated energy for retrofitted and corresponding specimen in virgin state is presented in Fig. 10. During all loading steps, both retrofitting solutions have provided a cumulative dissipated energy higher than the one registered in their corresponding virgin state. In this respect, the retrofitting solution applied in JPB specimen was more effective. In fact, at 4% of drift the cumulative dissipated energy of JPA3-R was 44.4 kN·m, which was only 5% larger than the corresponding value in JPA3, while the JPB-R reached 53.4 kN·m indicating an increase of 95% comparing to value calculated for JPB.

3.5. Secant stiffness

Degradation in the stiffness of a beam–column joint can progressively occurs when it is subjected to reversal cyclic loading. To assess the stiffness degradation, the secant stiffness, K_s, is estimated during the drift evolution, and its relationship is represented in Fig. 11, for both the specimen in the retrofitted and virgin states. The secant stiffness is taken as the slope of the straight line which connects the peak loads at the positive and the negative displacements of the load *versus* displacement envelop at the first cycle of each level of imposed drift. According

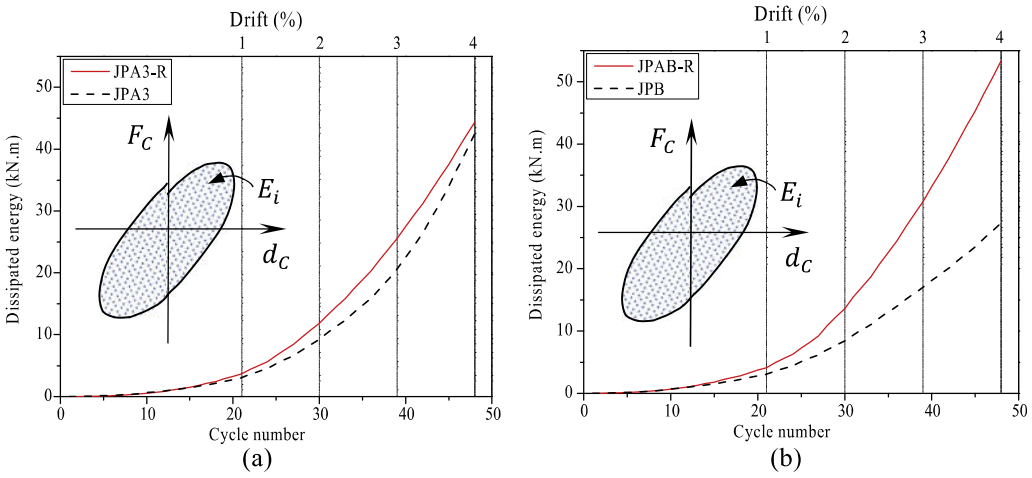

Fig. 10. Evolution of the dissipated energy during the cyclic loading (a) JPA3-R and JPA3, and (b) JPB-R and JPB.

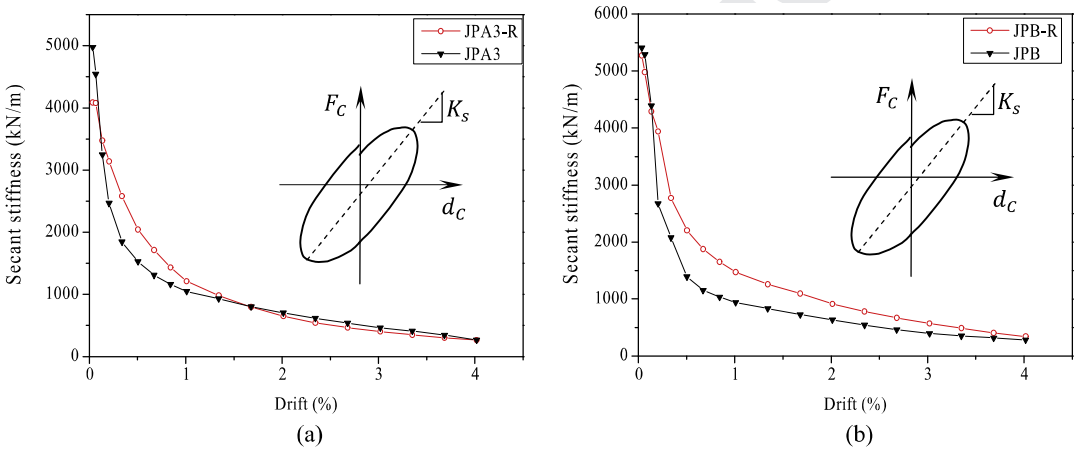

Fig. 11. Secant stiffness evolution in (a) JPA3-R and JPA3, and (b) JPB-R and JPB.

to this figure, the retrofitting technique adopted for JPA3-R has just restored 82% of the initial secant stiffness of this specimen in its virgin state, while the technique applied on the JPB-R has almost restored the initial secant stiffness registered in JPB (its virgin state). This can be explained by a less effective bond between the casted mortar and the old concrete of JPA3-R.

Considering the degradation of the secant stiffness at the end of each sets of loading cycles, JPA3-R had greater secant stiffness than JPA3 between loading cycles corresponds to 0.13% and 1.67%. After 1.67% the secant stiffness of the retrofitted and virgin state was fairly similar. For the case of JPB-R, after 0.13% of drift, the adopted retrofitting scheme resulted in a slower degradation in secant stiffness than its virgin state.

3.6. Displacement ductility

Ductility is the potential of a lateral load resisting system to undergo large inelastic deformation during its post-peak regime with only slight reduction in its ultimate lateral load carrying capacity. The ductility is generally quantified as a normalized displacement or a rotation index depending if the ductility is aimed to be assessed in terms of global or local behavior, respectively. For the case of the present study, the displacement ductility index (μ_Δ) is calculated as the ratio of the ultimate lateral displacement (d_u) and the displacement at the yield point (d_y), Fig. 12. The ultimate point can be defined as the displacement corresponding to a load level in the post-peak response of the specimen that is a fraction of the peak load (F_p). According to the available literature, this ratio can be taken between 10% and 20% [26–28]. The yield displacement can be obtained from a bi-linear curve

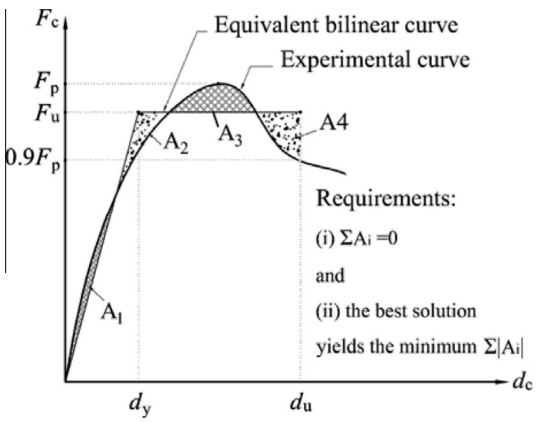

Fig. 12. Schematic representation of the definition of the equivalent bilinear curve for the evaluation of the displacement ductility index.

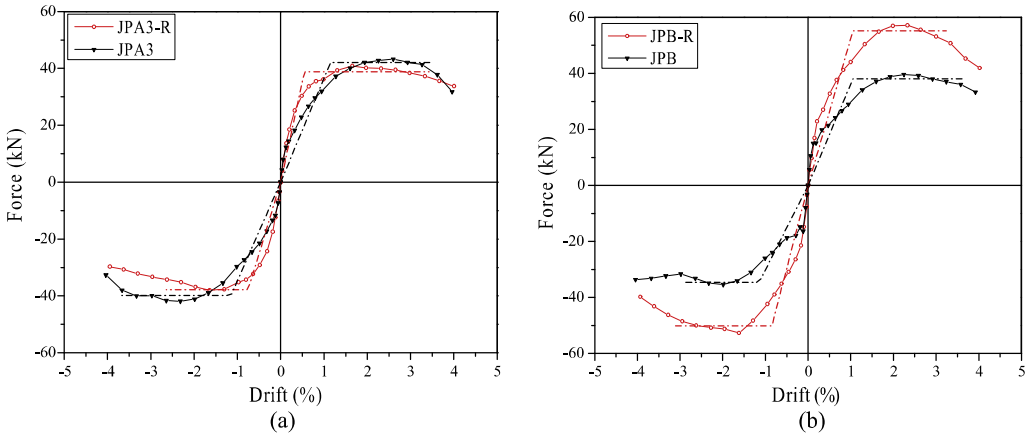

Fig. 13. Envelope of the load *versus* drift for both the repaired and virgin specimens along with the equivalent elastic–perfectly plastic curves (a) JPA3-R and JPA3, and (b) JPB-R and JPB.

Table 3
Data for the evaluation of displacement ductility factor.

Specimen	Negative direction		Positive direction		μ_Δ	$\left(\frac{\mu_\Delta^R-\mu_\Delta^V}{\mu_\Delta^V}\right)$
	d_y^- (mm)	d_u^- (mm)	d_y^+ (mm)	d_u^+ (mm)		
JPA3-R	−22.5 (−0.75)*	−79.2 (−2.64)	+16.5 (+0.55)	+102.9 (+3.43)	4.88	+56%
JPA3	−34.5 (−1.15)	−110.5 (−3.68)	+34.5 (+1.15)	+105.2 (+3.51)	3.13	
JPB-R	−25.5 (−0.85)	−93.3 (−3.11)	+31.5 (+1.05)	+97.2 (+3.24)	3.37	+12%
JPB	−34.5 (−1.15)	−87.6 (−2.92)	+31.5 (+1.05)	+108.9 (+3.63)	3.00	

* Values in parentheses indicate the corresponding drift in percentage at maximum bending moment.

assuming equivalent elastic–perfectly plastic response. To estimate this bi-linear curve, two conditions should be fulfilled: (i) the area under this curve should be equal to the one of the envelope of load *versus* lateral displacement, and (ii) the deviation between these two curves, measured based on the absolute sum of the areas enclosed between these curves, should be the minimum (see Fig. 12). The displacement ductility index is then calculated as the ratio between the ultimate and the yield displacements. In this context it was assumed for the ultimate displacement the one corresponding to 10% loss of the peak load ($0.9F_p$). The envelope of the load *versus* drift, and also the equivalent elastic–perfectly plastic curves estimated for both the retrofitted and virgin specimens are presented in Fig. 13. Table 3 also indicates the yield and the ultimate displacements obtained for the calculation of the displacement ductility index for the positive and negative loading, where μ_Δ^V and μ_Δ^R are the ductility for the specimen in the virgin and retrofitted state, respectively. The reported ductility index is calculated as the average ductility using the corresponding values of displacement ductility in both positive and negative displacements. It is verified that, for both retrofitted specimens the average of the yield displacements, in negative and positive directions, has decreased when compared to the average value registered for their corresponding specimens in the virgin state. The reduction of the yield displacement is a consequence of lower stiffness degradation assured by the retrofitting system, mainly during the cycles up to 1.15% of drift. According to the results included in Table 3, and comparing to the displacement ductility registered in the specimens in its virgin state, the retrofitting strategy has assured an increase of 56% and 12% in displacement ductility of JPA3-R and JPB-R, respectively. The higher increase in displacement ductility of JPA3-R can be attributed to the larger sliding between the retrofitting scheme and the concrete substrate, and also due to the existence of larger damages before retrofitting of this specimen.

4. Conclusions

The effectiveness of retrofitting methodologies by jacketing the critical regions of two full-scale severely damaged reinforced concrete (RC) interior beam–column joints was experimentally investigated. Cast-in-place strain hardening cement composites (SHCC) reinforced with carbon fiber reinforced polymer (CFRP) laminates according to the near surface mounted (NSM) technique forms the main concept of the adopted retrofitting strategy. Two variations of this retrofitting technique were applied, where the main difference is restricted to the number of the retrofitted sides of the sections of the elements (2 sides in the JPA3-R and 4 sides in JPB-R specimens). Chemical anchors were used to improve shear stress transference between retrofitting scheme and the existing concrete substrate.

The developed SHCC was able to easily flow and fill the relatively small gaps between formworks and the substrate without the need of any vibration, which is an important requisite for a cast in place retrofitting intervention. Based on the results obtained from experimental tests where cyclic lateral loading under a constant column axial force was applied, the following conclusions can be pointed out:

1. Two-sided retrofitting system applied to the severely damaged JPA3 specimen was capable of restoring the lateral load carrying capacity and energy dissipation performance, and increase the ductility registered in the virgin state of this specimen. The initial secant stiffness of this specimen in its virgin state was, however, not totally recovered (82%).
2. The four-sided retrofitting system applied in the severely damaged JPB specimen assured a significant increase in terms of lateral load capacity and energy dissipation when the corresponding values registered in this specimen in its virgin

Please cite this article in press as: Esmaeeli E et al. Retrofitting of interior RC beam–column joints using CFRP strengthened SHCC: Cast-in-place solution. Compos Struct (2014), http://dx.doi.org/10.1016/j.compstruct.2014.12.012

state are considered for comparison purposes. A higher increase of the flexural resistance for the beams was also obtained due to the presence of CFRP laminates in the top and bottom faces of the beams, which has contributed to decrease the sliding of the flexural steel reinforcement of these beams. This technique has also decreased the rate of the stiffness degradation during the cyclic loading process, and assured a higher increase of ductility than the two-sided retrofitting configuration. In comparison with the substantial enhancement attained for these mentioned seismic characters, the increase in displacement ductility was only 12%.

3. Although the governing failure mode for both specimens was joint shear capacity deterioration, no brittle response was observed.
4. Considering that the progress of the inclined cracks in the joint region resulted in debonding failure between the adhesive of the X-shaped CFRP laminates and the SHCC, effectiveness of this configuration of CFRP laminates in the joint region is under question. Therefore, bonding a horizontal or vertical arrangement of transverse CFRP laminates at this region is recommended.
5. A high capacity of stress redistribution in SHCC resulted in multiple crack formation around anchored regions, but no bearing failure was observed.
6. The final geometry of the retrofitted specimens was almost not affected by the proposed retrofitting interventions, but the seismic performance of these specimens was significantly improved.

Acknowledgments

The study presented in this paper is a part of the research project titled "PrePam–Pre-fabricated thin panels by using advanced materials for structural rehabilitation" with reference number of PTDC/ECM/114511/2009. The first author acknowledges the grant SFRH/BD/65663/2009 provided by FCT. The authors also thank the collaboration of the following material suppliers: SIKA, Dow Chemical Co., ENDESA Compostilla Power Station, S&P, Hilti, and also Artecanter for transportation of the specimens.

References

[1] Hakuto S, Park R, Tanaka H. Seismic load tests on interior and exterior beam–column joints with substandard reinforcing details. ACI Struct J 2000;97:15.
[2] Pampanin S, Calvi GM, Moratti M. Seismic behaviour of R.C. beam–column joints designed for gravity loads. In: 12th European conference on earthquake engineering. London: Elsevier Science Ltd; 2002.
[3] Tsonos AG. Effectiveness of CFRP-jackets and RC-jackets in post-earthquake and pre-earthquake retrofitting of beam–column subassemblages. Eng Struct 2008:30.
[4] Tsonos A-DG. Performance enhancement of R/C building columns and beam–column joints through shotcrete jacketing. Eng Struct 2010:32.
[5] Karayannis CG, Sirkelis GM. Strengthening and rehabilitation of RC beam–column joints using carbon-FRP jacketing and epoxy resin injection. Earthquake Eng Struct Dyn 2008:37.
[6] Esmaeeli E, Danesh F. Shear strengthening of 3D corner beam–column connection using bidirectional GFRP layers. In: Motavalli M, editor. Proceeding of fourth international conference on FRP composites in civil engineering (CICE2008). Zurich, Switzerland: International Institute for FRP in Construction (IIFC); 2008.
[7] Danesh F, Esmaeeli E, Alam MF. Shear strengthening of 3D RC beam–column connection using GFRP: FEM study. Asian J Appl Sci 2008:1.
[8] Ha G-J, Cho C-G, Kang H-W, Feo L. Seismic improvement of RC beam–column joints using hexagonal CFRP bars combined with CFRP sheets. Compos Struct 2013:95.
[9] Lee WT, Chiou YJ, Shih MH. Reinforced concrete beam–column joint strengthened with carbon fiber reinforced polymer. Compos Struct 2010:92.
[10] Esmaeeli E, Barros JAO, Baghi H. Hybrid composite plates (HCP) for shear strengthening of RC beams. In Minho Uo, editor. 11th international symposium on fiber reinforced polymers for reinforced concrete structures (FRPRCS11), Guimaraes; 2013. p. 11–4.
[11] Shannag MJ, Alhassan MA. Seismic upgrade of interior beam–column subassemblages with high-performance fiber-reinforced concrete jackets. ACI Struct J 2005;102:8.
[12] Wang Y-C, Hsu K. Shear strength of RC jacketed interior beam–column joints without horizontal shear reinforcement. ACI Struct J 2009;106:11.
[13] Esmaeeli E, Manning E, Barros JAO. Strain hardening fibre reinforced cement composites for the flexural strengthening of masonry elements of ancient structures. Constr Build Mater 2013;38:1010–21.
[14] Esmaeeli E, Barros JAO, Baghi H, Sena-Cruz J. Development of hybrid composite plate (HCP) for the repair and strengthening of RC elements. In: 3rd international RILEM conference on strain hardening cementitious composites (SHCC3-Delft). Dordrecht, Netherlands: RILEM Publications SARL; November 3–5, 2014.
[15] Lim YM, Li VC. Durable repair of aged infrastructures using trapping mechanism of engineered cementitious composites. Cem Concr Compos 1997:19.
[16] Sahmaran M, Li M, Li VC. Transport properties of engineered cementitious composites under chloride exposure. ACI Mater J 2007:104.
[17] Rokugo K, Kunieda M, Lim S. Patching repair with ECC on cracked concrete surface. In Proc of ConMat05, Vancouver, Canada [CD-ROM]; 2005.
[18] Kobayashi K, Iizuka T, Kurachi H, Rokugo K. Corrosion protection performance of high performance fiber reinforced cement composites as a repair material. Cem Concr Compos 2010:32.
[19] Sahmaran M, Li VC, Andrade C. Corrosion resistance performance of steel-reinforced engineered cementitious composite beams. ACI Mater J 2008:105.
[20] Fernandes CAL. Cyclic behaviour of RC elements with plain reinforcing bars [PhD]. Aveiro, Portugal: University of Aveiro; 2012.
[21] EN1992-1-1. Eurocode 2: Design of Concrete Structures. Part 1–1: General Rules and Rules for Buildings. Brussels, Belgium: European Committee for Standardization; 2004.
[22] Esmaeeli E, Barros J, Mastali M. Effects of curing conditions on crack bridging response of PVA reinforced cementitious matrix. In 8th RILEM international symposium on fibre reinforced concrete: challenges and opportunities (BEFIB2012). Guimaraes, Portugal; 2012.
[23] Costa IG, Barros JAO. Evaluation of the influence of adhesive properties and geometry of carbon fiber laminates using pull-out tests. Department of Civil Engineering, University of Minho; 2012. p. 16.
[24] International Organization for Standardization – ISO 527–2:1996. Plastics – Determination of tensile properties – Part 2: Test conditions for moulding and extrusion plastics. London South Bank University.
[25] Verderame GM, Fabbrocino G, Manfredi G. Seismic response of R.C. columns with smooth reinforcement. Part II: Cyclic tests. Eng Struct 2008:30.
[26] Paulay T. Equilibrium criteria for reinforced concrete beam–column joints. ACI Struct J 1989;86:8.
[27] EN 1998–3. Eurocode 8: Design of structures for earthquake resistance – Part 3: Assessment and retrofitting of buildings; 2005.
[28] Fardis M, Biskinis D. Deformation capacity of R.C. members, as controlled by flexure or shear. In: Performance based engineering for earthquake resistant reinforced concrete structures: a volume honoring Shunsuke Otani. University of Tokyo; 2003.